Comparison of two methodologies for calibrating satellite instruments in the visible and near infrared

Robert A. Barnes[a]*, Steven W. Brown[b], Keith R. Lykke[b], Bruce Guenther[c], Xiaoxiong (Jack) Xiong[d], James J. Butler[d]

[a]Science Applications International Corporation, Beltsville, MD 20705
[b]National Institute of Standards and Technology, Gaithersburg, MD 20899
[c]National Oceanic and Atmospheric Administration, Silver Spring, MD 20910
[d]NASA Goddard Space Flight Center, Greenbelt, MD 20771

ABSTRACT

Traditionally, satellite instruments that measure Earth-reflected solar radiation in the visible and near infrared wavelength regions have been calibrated for radiance response in a two-step method. In the first step, the spectral response of the instrument is determined using a nearly monochromatic light source, such as a lamp-illuminated monochromator. Such sources only provide a relative spectral response (RSR) for the instrument, since they do not act as calibrated sources of light nor do they typically fill the field-of-view of the instrument. In the second step, the instrument views a calibrated source of broadband light, such as a lamp-illuminated integrating sphere. In the traditional method, the RSR and the sphere spectral radiance are combined and, with the instrument's response, determine the absolute spectral radiance responsivity of the instrument. More recently, an absolute calibration system using widely tunable monochromatic laser systems has been developed. Using these sources, the absolute spectral responsivity (ASR) of an instrument can be determined on a wavelength-by-wavelength basis. From these monochromatic ASRs, the responses of the instrument bands to broadband radiance sources can be calculated directly, eliminating the need for calibrated broadband light sources such as integrating spheres. Here we describe the laser-based calibration and the traditional broad-band source-based calibration of the NPP VIIRS sensor, and compare the derived calibration coefficients for the instrument. Finally, we evaluate the impact of the new calibration approach on the on-orbit performance of the sensor.

Keywords: NPP VIIRS, radiance, prelaunch calibration

1. INTRODUCTION

The Visible Infrared Imaging Radiometer Suite (VIIRS) for the National Polar-orbiting Operational Environmental Satellite System (NPOESS) Preparatory Project (NPP) is a 22-band sensor with nine spectral bands in the visible and near infrared, eight spectral bands in the short-wave and mid-wave infrared, and four bands in the long-wave infrared[1]. The wavelengths for the spectral bands extend from 412 nm to 12.013 μm (ref. 2). NPP VIIRS and the successor VIIRS instruments are designed to provide data continuity with the Moderate-resolution Imaging Spectroradiometers (MODIS) from the National Aeronautics and Space Administration's (NASA's) Earth Observing System (EOS)[3]. NPP VIIRS incorporates a substantial hardware heritage from MODIS, particularly for its calibration subsystems[1,4], which are MODIS flight-proven designs. The on-orbit and prelaunch calibrations of NPP VIIRS follow those of the MODIS instruments closely. For measurements on orbit, the principal data product from the sensor is reflectance, using the solar diffuser as the onboard calibration reference. For the laboratory calibration, the spectral responses for the visible and near infrared bands are characterized during thermal-vacuum (TVAC) testing[2]. Also, during TVAC testing VIIRS views the integrating sphere (or spherical integrating source, SIS) that was also used for the calibration of MODIS[5]. That source, the SIS100[2], is the prelaunch calibration standard for VIIRS. The SIS100 radiances, combined with the VIIRS sensor bands' pre-TVAC relative spectral responses, provide calibrated band-averaged radiance responsivities for the visible and near infrared bands. For the NPP VIIRS sensor, as with the MODIS sensors before, the required calibration uncertainty for radiance measurements is 5 % or less; for reflectance measurements it is 2 % or less.

*(RAB, contact author) Robert.A.Barnes@nasa.gov; phone (301) 286-0501; facsimile (301) 286-0268; Ocean Biology Processing Group, Mail Code 614.8, NASA Goddard Space Flight Center, Greenbelt, MD 20771

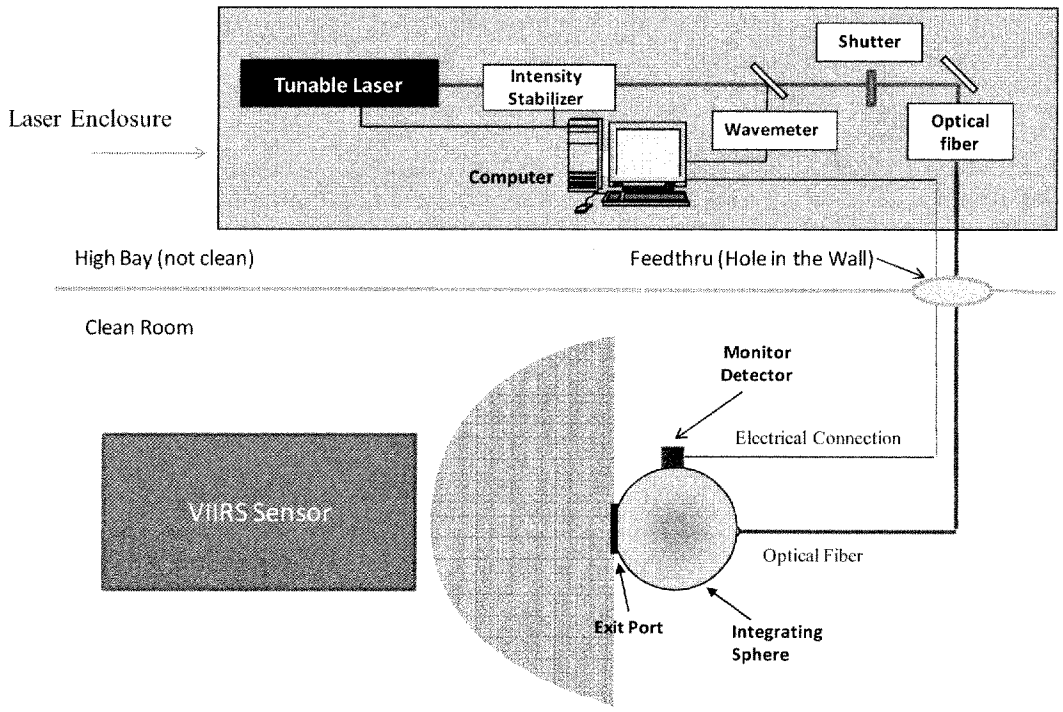

Figure 1. Measurement setup for the SIRCUS measurements at BATC. The VIIRS sensor views calibrated monochromatic radiance from the exit port of the integrating sphere. Additional details are given in the text.

Over the past decade there has been the development of a new radiometric calibration capability at the National Institute of Standards and Technology (NIST). This capability, the Facility for Spectral Irradiance and Radiance Responsivity Calibrations Using Uniform Sources (SIRCUS)[6], incorporates wavelength-tunable lasers coupled into spherical integrating sources plus detectors, traceable to primary standards at NIST, as calibrated reference standards. There are two principal advantages to using the laser-based source approach over the conventional lamp-illuminated integrating sphere approach. First, the sensor's entrance pupil can be uniformly filled using the laser-based sources. With the conventional approach, the radiant flux from the lamp-monochromator system used to determine the sensor's RSR typically underfills the instrument's field-of-view due to signal-to-noise limitations. Second, the radiance of the SIS at each wavelength is known with very low uncertainties, 20 % or less of the uncertainty in the broad-band SIS radiance. These advantages offer the possibility of calibrating satellite sensors with lower uncertainty than is possible using historical calibration approaches.

To evaluate the potential of the new calibration approach for satellite sensors, the NPP Project management group at NASA's Goddard Space Flight Center (GSFC) and the Integrated Program Office (IPO) at the National Oceanic and Atmospheric Administration (NOAA) funded a special test of NPP VIIRS using a portable version of SIRCUS at the facility of the NPP spacecraft manufacturer (Ball Aerospace and Technologies Corporation, BATC) in early 2010. This test was performed immediately after the integration of the completed flight instrument onto the spacecraft platform. In the following sections, we describe the instrument band responsivities from the TVAC testing at the instrument manufacturer's facility and from the special test at the spacecraft manufacturer's facility. The comparison of these two sets of band responsivities also requires a discussion of the out-of-band components of the VIIRS spectral responses and their effects on the dependence of the outputs of the bands to the spectral shapes of the radiances viewed.

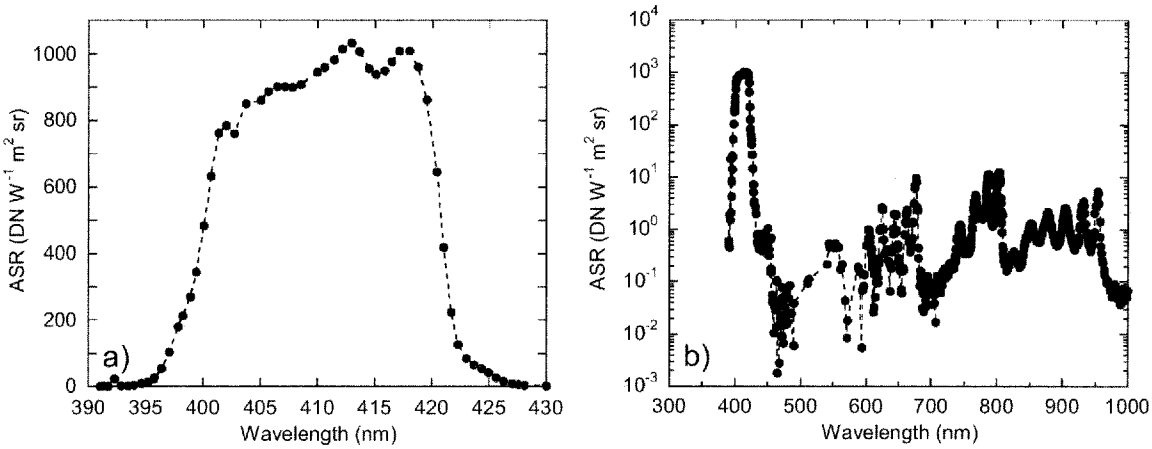

Figure 2. Absolute Spectral Responses for detector 8 of NPP VIIRS band M1 (411 nm). The symbols show the individual measurements.

a) Band M1 ASRs near the central peak.

b) Band M1 ASRs for the full set of measurements.

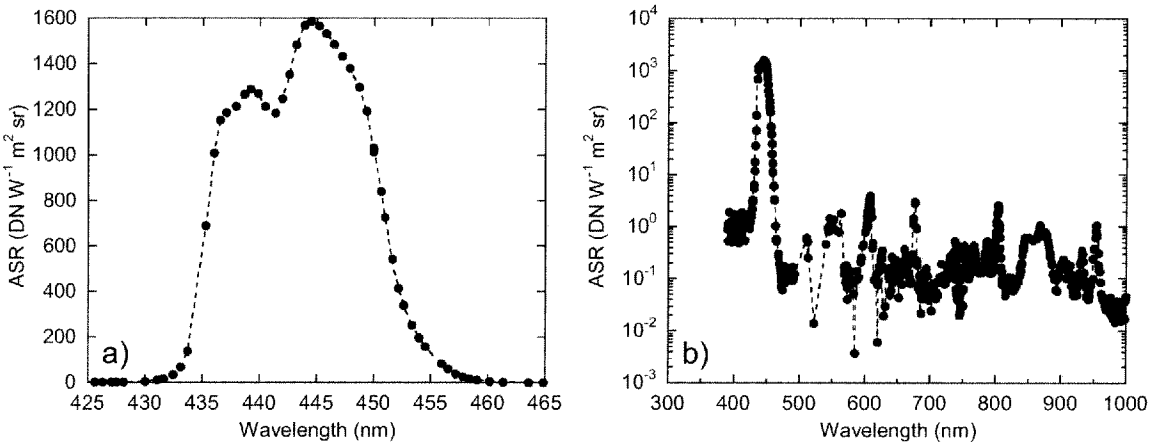

Figure 3. Absolute Spectral Responses for detector 8 of NPP VIIRS band M2 (444 nm). The symbols show the individual measurements.

a) Band M2 ASRs near the central peak.

b) Band M2 ASRs for the full set of measurements.

2. TRAVELING SIRCUS AT BALL AEROSPACE

The SIRCUS facility at NIST has been described in detail previously (Brown et al.,2006); a similar configuration was used during VIIRS sensor testing at BATC, Fig. 1. The SIRCUS setup provided monochromatic radiance from a 76.2 cm diameter integrating sphere equipped with a 25.4 cm diameter aperture. The integrating sphere was aligned to the VIIRS sensor nadir (Earth-view) port in the BATC clean room. It was illuminated by high-power tunable lasers kept in the high bay area outside the clean room. Radiant flux from the laser sources was coupled to the SIS using steel-jacketed 200 μm core diameter silica-silica optical fiber. A beamsplitter in the optical path sent a small portion of the laser radiation into a wavemeter that measured the wavelength of the radiation. An electronic shutter in the optical path could be remotely controlled, allowing ambient signal levels to be routinely acquired. During testing, the VIIRS telescope was fixed to view the output from the SIS, and VIIRS continuously acquired data. The shutter was closed while the wavelength was changed, providing a beginning and end of wavelength dark signal in the VIIRS data. These ambient signals, combined with timestamps in the data sets were critical for properly merging SIRCUS and VIIRS data sets.

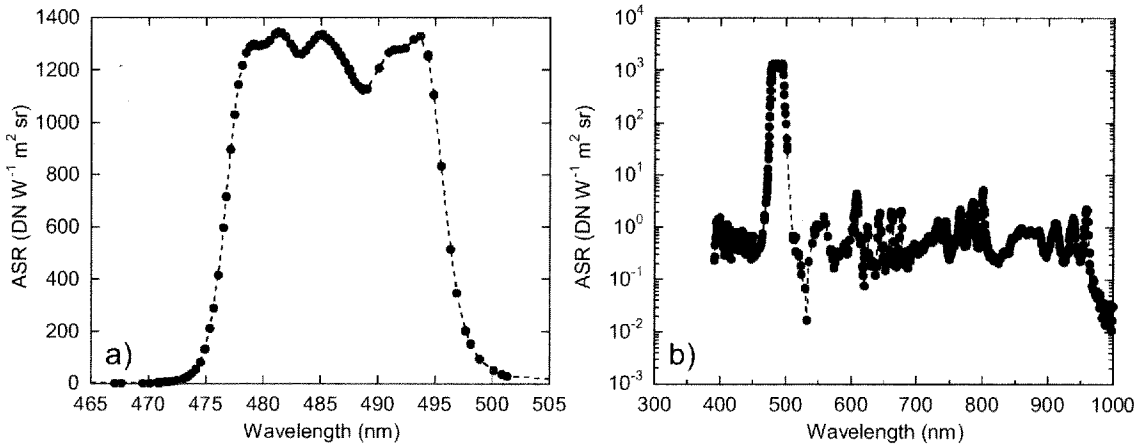

Figure 4. Absolute Spectral Responses for detector 8 of NPP VIIRS band M3 (486 nm). The symbols show the individual measurements.

a) Band M3 ASRs near the central peak.

b) Band M3 ASRs for the full set of measurements.

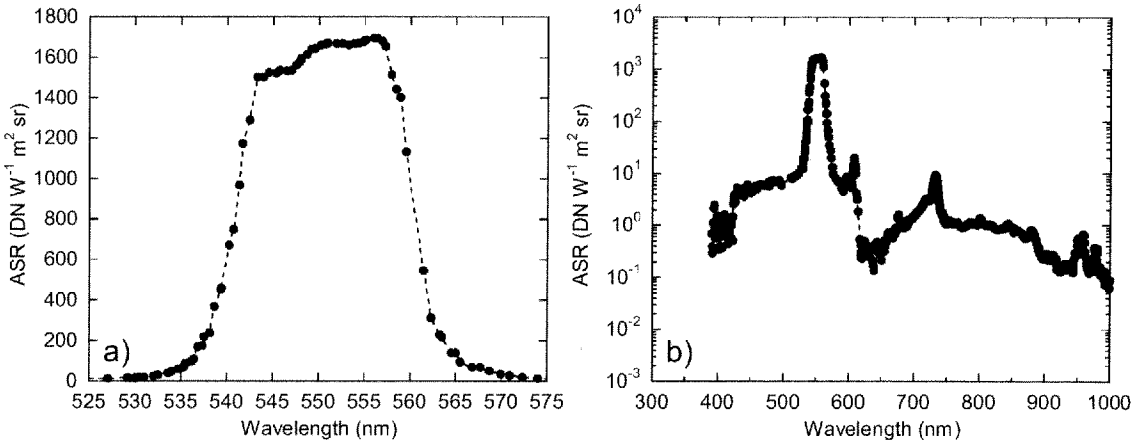

Figure 5. Absolute Spectral Responses for detector 8 of NPP VIIRS band M4 (551 nm). The symbols show the individual measurements.

a) Band M4 ASRs near the central peak.

b) Band M4 ASRs for the full set of measurements.

Two radiance meters calibrated at the NIST SIRCUS facility were used at BATC to provide a calibration of two silicon photodiodes mounted on the sphere wall. The calibration related the monitor signal to the sphere radiance. The sphere-mounted photodiodes were calibrated pre- and post-VIIRS measurements in the BATC high bay outside the clean room. During VIIRS measurements of the sphere, the radiance was determined solely by the monitor detectors. The uncertainty for the SIRCUS radiances at BATC is estimated to be 0.5 %.

During a measurement sequence, the SIRCUS computer recorded time, wavelength, and the signals from the two sphere mounted photodiodes. Concurrently, time and the digital numbers (DNs) from the satellite instrument were recorded by the instrument's ground support equipment. The DNs from the dark periods were subtracted to provide the net DNs for each radiance level from the sphere. The result at each laser wavelength was the net DNs for each VIIRS band and detector divided by the monochromatic radiance from the sphere, giving an Absolute Spectral Response (ASR).

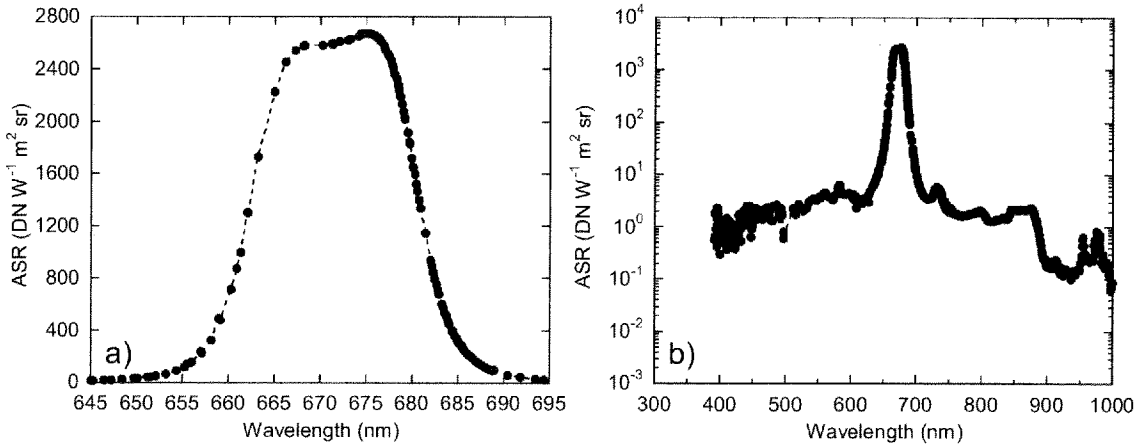

Figure 6. Absolute Spectral Responses for detector 8 of NPP VIIRS band M5 (672 nm). The symbols show the individual measurements.

a) Band M5 ASRs near the central peak.

b) Band M5 ASRs for the full set of measurements.

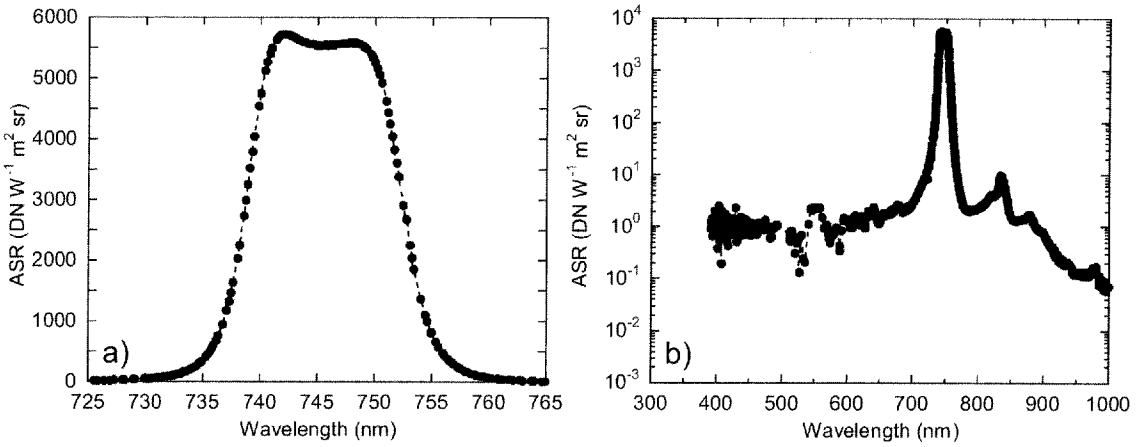

Figure 7. Absolute Spectral Responses for detector 8 of NPP VIIRS band M6 (746 nm). The symbols show the individual measurements.

a) Band M6 ASRs near the central peak.

b) Band M6 ASRs for the full set of measurements.

2.1. SIRCUS-based Absolute Spectral Responses.

The ASRs for VIIRS band M1, detector 8, are shown in Fig. 2. Detector 8 is located at the center of the set of 16 detectors aligned on the focal plane in the direction of flight of VIIRS. The symbols in the figure show the calibration coefficients derived from individual measurements. Fig. 2a shows the spectral responses near the central peak for band M1. The panel has a linear ordinate. The full set of ASRs for band M1 are shown in Fig. 2b with a logarithmic ordinate. Negative responses and duplicate measurements, that is, multiple measurements at a given wavelength, have been removed from the data set. The ASRs for band M2 in panels a and b of Fig. 3 follow the same format as those for band M1 in Fig. 2. In a similar manner, the ASRs for bands M3 through M7 are shown in Figs. 4 through 8.

3. SIRCUS-BASED RESPONSIVITIES, BANDWIDTHS, AND CENTER WAVELENGTHS

For NPP VIIRS, the instrument output is in digital numbers (DN). For each measurement, the radiance from the SIRCUS sphere, in W m^{-2} sr^{-1}, and the VIIRS DNs are combined to give an absolute spectral response (ASR), in DN (W m^{-2} sr^{-1})$^{-1}$, at the wavelength measured by the wavemeter (in nm). The units for the monochromatic ASR can

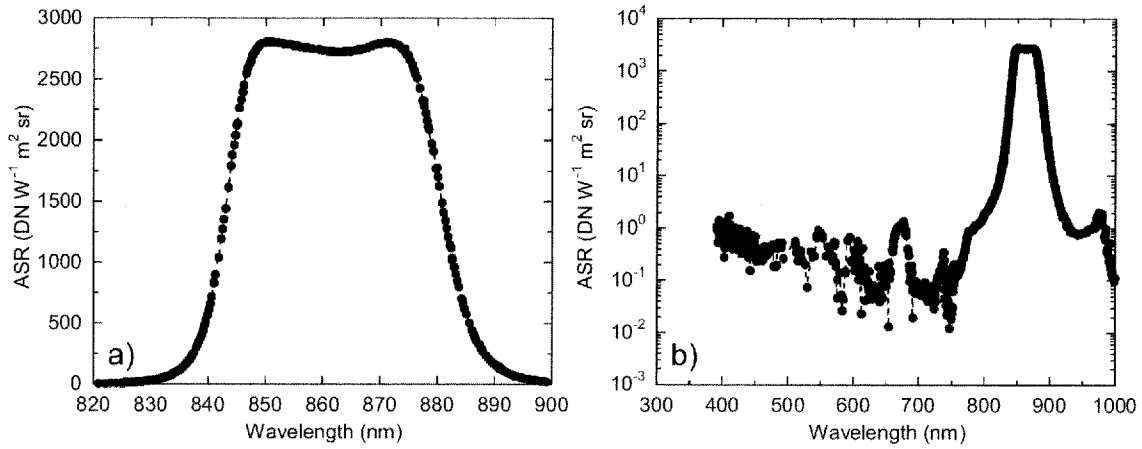

Figure 8. Absolute Spectral Responses for detector 8 of NPP VIIRS band M7 (862 nm). The symbols show the individual measurements.

a) Band M7 ASRs near the central peak.

b) Band M7 ASRs for the full set of measurements.

also be written as DN W^{-1} m^2 sr. The responsivity for the band is the integration of the monochromatic ASRs in the measurement set. For band M1, for example, it is the area under the curve in Fig. 2b. The integration can be done as a trapezoidal summation

$$Band\ Responsivity = \sum_{n=2}^{nmax} \frac{ASR(n) + ASR(n-1)}{2} \left[\lambda(n) - \lambda(n-1) \right] , \tag{1}$$

where ASR(n), the ordinate, is the monochromatic ASR for measurement n, and $\lambda(n)$, the abscissa, is the wavelength for that measurement. Note that the wavelength interval in Eq. 1 is not constant, as the data were not acquired with a constant wavelength spacing. The units for the band responsivity are DN W^{-1} m^2 sr nm, where the nm in the units derives from the sum of the $\Delta\lambda$ terms in the abscissa portions of the individual trapezoids. The band responsivity is often called the gain for the band.

It is also possible to interpolate the monochromatic ASRs to a set of constant wavelength intervals. This allows an integration using the sums of histograms

$$Band\ Responsivity = \sum_{\lambda=390}^{\lambda=1000} ASR(\lambda) \Delta\lambda , \tag{2}$$

where $\Delta\lambda$ is the wavelength spacing between interpolated ASRs. The summation covers the wavelength range of the measured ASRs, 390 nm to 1000 nm. Using a spacing of 0.1 nm is convenient for spectral responses. A comparison between the band responsivities derived using a trapezoidal summation and a histogram summation shows agreement between the two approaches to 2 parts in one hundred thousand.

The interpolation technique used for Eq. 2 allows the calculation of additional data products, in particular, the center wavelength and the bandwidth for the responsivity. These are determined through the technique of band-averaging. The band-averaged center wavelength, λ_C, is given by Eq. 3,

$$\lambda_c = \frac{\sum_{\lambda=390}^{\lambda=1000} \lambda\, ASR(\lambda) \Delta\lambda}{\sum_{\lambda=390}^{\lambda=1000} ASR(\lambda) \Delta\lambda} , \tag{3}$$

When the denominator of Eq. 3 is normalized to a maximum of unity through division by the maximum ASR, the summation in the denominator of Eq. 3 becomes the bandwidth, bw,

$$bw = \sum_{\lambda=390}^{\lambda=1000} \frac{ASR(\lambda)}{ASR_{MAX}} \Delta\lambda = \frac{1}{ASR_{MAX}} \sum_{\lambda=390}^{\lambda=1000} ASR(\lambda) \Delta\lambda , \tag{4}$$

Table 1. Center wavelengths, bandwidths, maximum absolute spectral responses and band responsivities for NPP VIIRS bands M1 through M7. Only detector 8 for each band is used in this study. The center wavelength is calculated over the central peak of each band at the 1 % response limit, and the maximum ASR is taken from each response spectrum by inspection. The trapezoidal band responsivities are calculated using Eq. 1, and the histogram responsivities are calculated using Eq. 2. The two sets of responsivities agree at the 0.002 % level.

VIIRS Band	Center Wavelength (nm)	Bandwidth (nm)	Max ASR (DN W^{-1} m^2 sr)	Trapezoidal Responsivity (DN W^{-1} m^2 sr μm)	Histogram Responsivity (DN W^{-1} m^2 sr μm)
M1	410.6	19.889	1033.584	20.5565	20.5566
M2	443.6	14.296	1586.286	22.6764	22.6768
M3	486.4	19.201	1347.509	25.8731	25.8734
M4	550.8	20.763	1698.208	35.2593	35.2593
M5	671.6	19.975	2674.079	53.4140	53.4138
M6	745.6	14.550	5719.537	83.2177	83.2178
M7	862.1	39.178	2809.293	110.0638	110.0628

where bw has units of the spacing between interpolated measurements. In this case the spacing is 0.1 nm, so the summed results from Eq. 4 must be divided by ten to obtain the bw values in Table 1. The division in Eq. 4 also converts the ASRs at individual wavelengths to relative spectral responses (RSRs). In addition, Eq. 4 shows the relationship between the band responsivity, the maximum ASR, and the bandwidth

$$Band\ Responsivity = \sum_{\lambda=390}^{\lambda=1000} ASR(\lambda)\Delta\lambda = bw\,ASR_{MAX} \quad , \tag{5}$$

where the band responsivity is the product of the maximum ASR and the bandwidth.

A note on units: the radiance units for the band responsivities in Eq. 1 and Eq. 2 are W m^{-2} sr^{-1} nm^{-1}. For NPP VIIRS, the radiance units are given in terms of μm^{-1} instead of nm^{-1}. This requires a conversion factor of $1x10^{-3}$ to convert the band responsivities from DN W^{-1} m^2 sr nm to DN W^{-1} m^2 sr μm. It is the latter units that are used in the presentation of the results below.

The center wavelengths, bandwidths, maximum ASRs, and band responsivities for NPP VIIRS bands M1 through M7 are listed in Table 1. Only detector 8 for each band is used in this study, although measurements of all 16 detectors for each band were made at BATC. The center wavelength is calculated using Eq. 3; the bandwidth is calculated using Eq. 4; and the maximum ASR is taken from each response spectrum by inspection. The band responsivities for NPP VIIRS bands M1 through M7 are also listed in Table 1. The band responsivities derived from trapezoids are calculated using Eq. 1, and the band responsivities derived from histograms are calculated using Eq. 2. The units for the spectral radiances in Table 1 are those used for on-orbit measurements by VIIRS.

4. LAMP-MONOCHROMATOR-BASED RELATIVE SPECTRAL RESPONSE

For the laboratory calibration by the instrument manufacturer, the spectral responses for the VIIRS visible and near infrared bands were characterized during TVAC testing. For these bands, a lamp-illuminated double monochromator, the Spectral Measurement Assembly (SpMA), was used as a source of nearly monochromatic light, with a bandpass of 2 nm. The SpMA was also used in the spectral characterization of the bands for both MODIS instruments. For measurements of the quasi-monochromatic flux from the SpMA by VIIRS, there is a set of transition optics to focus the output of the SpMA onto the instrument's detectors. The SpMA uses an incandescent lamp for the visible and near infrared measurements. The lamp has a peak output near 1000 nm with significantly less flux at lower wavelengths. This causes a spectrally dependent shape in the output from the SpMA's monochromator. To correct for this effect, a reference detector with known quantum efficiency also views the flux from the SpMA. This is done before and after the VIIRS spectral response measurements. The reference detector does not share the transition optics used in the measurements by VIIRS, so the detector monitors the relative output of the SpMA with wavelength but not the absolute value of that output. The SpMA-based spectral responses for each VIIRS band, after correction for the spectral shape of the flux from the source, is normalized to the peak value for that band's response to give a relative spectral response (RSR). The lamp-monochromator system does not fill the field-of-view of the VIIRS sensor and is incapable of producing absolute spectral responses.

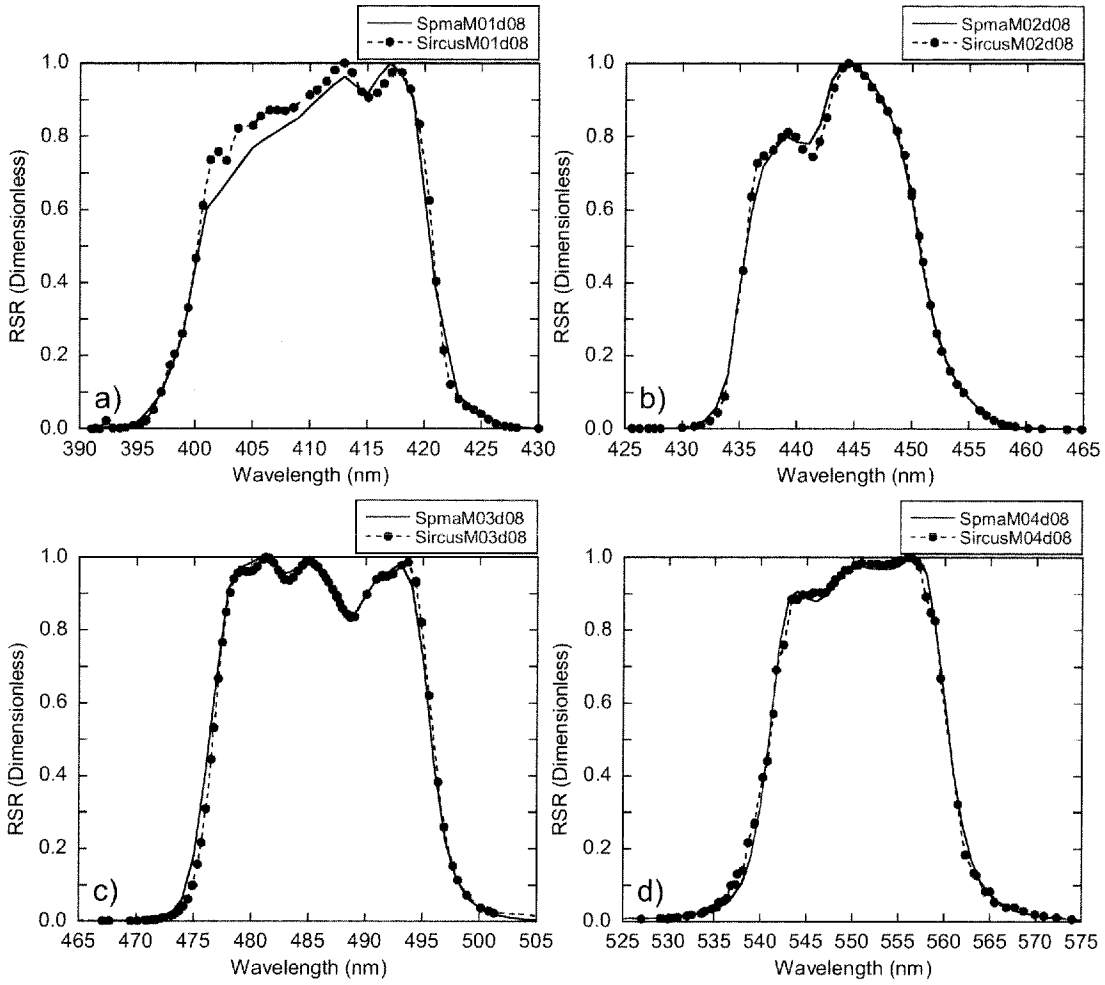

Figure 9. SIRCUS-based and SpMA-based relative spectral responses for detector 8 of NPP bands M1 through M4. The SpMA-based measurements were taken at 2 nm intervals. For the SIRCUS-based responses, the ASRs have been normalized to a maximum of unity. The panels show the responses near the central peaks.

a) Band M1 RSRs.
b) Band M2 RSRs.
c) Band M3 RSRs.
d) Band M4 RSRs.

The NPP VIIRS peak-normalized RSRs are shown in Figs. 9 and 10. They are for detector 8 of each band, the same detector selected for the presentation of the SIRCUS-based ASRs. The lamp-monochromator-based RSRs in Figs. 9 and 10 are given the designation "SpMA-based" in the legends for the panels. The SIRCUS-based RSRs in the figures are the ASRs from Figs. 2-8 normalized to their maximum values.

For band M1, there is an obvious difference in the spectral responses on the short wavelength side of the central peak. This is at the extreme wavelength range for the SpMA measurements, where the flux from the incandescent lamp illuminating the double monochromator is least. It is noteworthy that more than one of the SpMA incandescent lamps failed during the spectral measurements by the instrument manufacturer. The lamp failures are indications of basic problems with the lamps, possibly caused by age. In some cases, there were no measurements by the SpMA's reference detector before the failure of the lamp. Consequently, there is the distinct possibility of a drift in the SpMA lamp used for the measurement of VIIRS band M1 during the measurement process. Such a drift between the time that the SpMA was viewed by the reference detector and the time it was viewed by VIIRS could explain the differences observed in Fig. 8a for band M1.

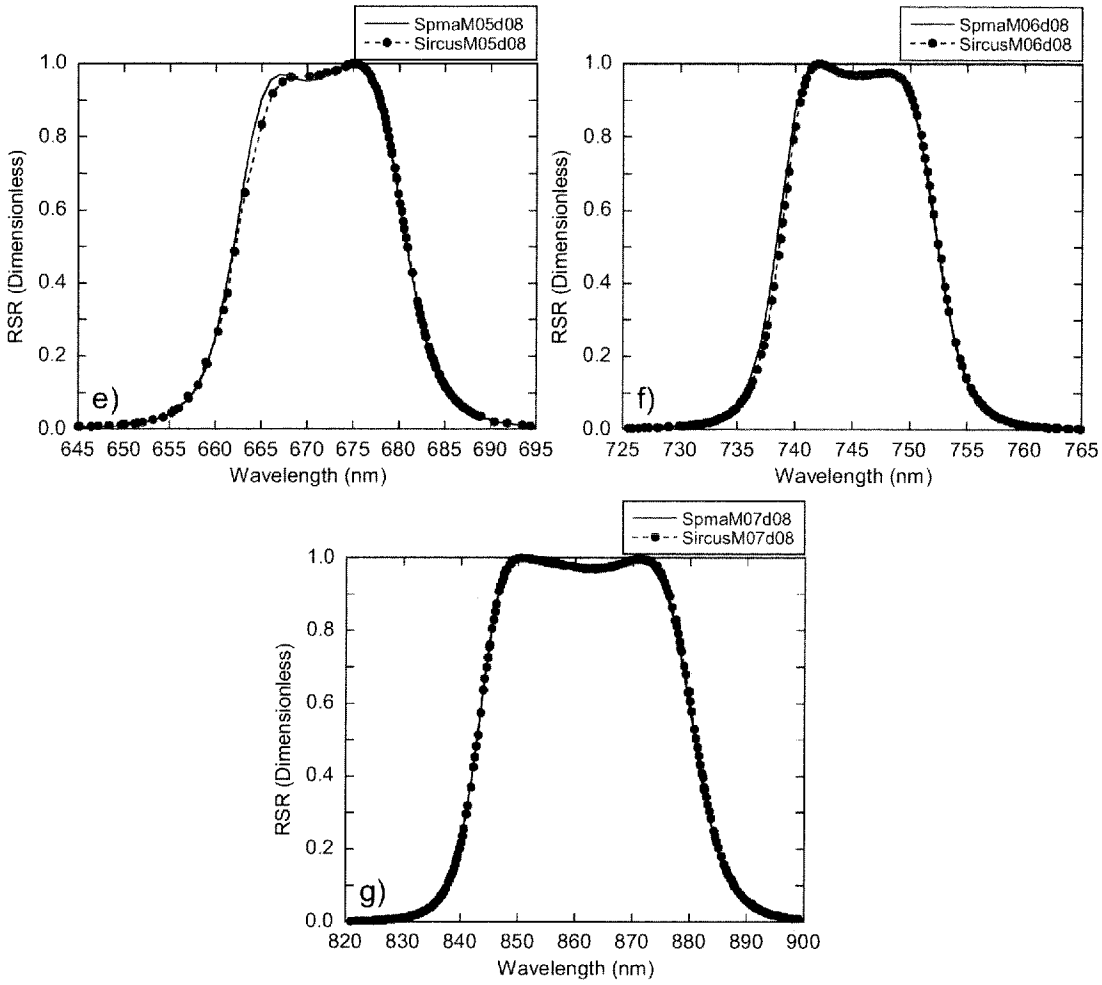

Figure 10. SIRCUS-based and SpMA-based relative spectral responses for detector 8 of NPP bands M5 through M7. The SpMA-based measurements were taken at 2 nm intervals. For the SIRCUS-based responses, the ASRs have been normalized to a maximum of unity. The panels show the responses near the central peaks.

e) Band M5 RSRs.
f) Band M6 RSRs.
g) Band M7 RSRs.

Table 2. Bandwidths using SIRCUS and the SpMA. The SIRCUS-based values come from the ASRs for each band divided by the maximum ASR. The SpMA-based values, also divided by the value for the peak, come from measurements during TVAC testing. The bandwidths are calculated using Eq. 4. The differences are the SpMA-based bandwidths from SIRCUS.

VIIRS Band	SIRCUS-based Bandwidth (nm)	SpMA-based Bandwidth (nm)	Difference (%)
M1	19.889	19.166	-3.6
M2	14.296	14.255	-0.3
M3	19.201	19.194	0.0
M4	20.763	20.709	-0.3
M5	19.975	20.186	1.1
M6	14.550	14.709	1.1
M7	39.178	38.901	-0.7

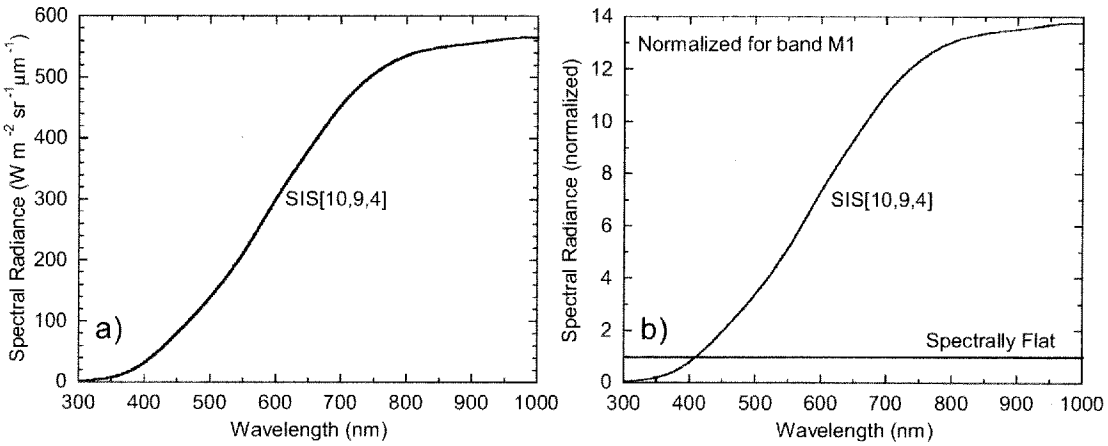

Figure 11 Radiance spectrum for one lamp level of the sphere used to calibrate Terra and Aqua MODIS. The sphere has ten 200 W, nine 45 W, and four 8 W lamps illuminated. This provides a proxy for the spectral shape of the sphere used to calibrate NPP VIIRS.

a) Sphere radiances in W m^{-2} sr^{-1} μm^{-1}.

b) Sphere radiances normalized to unity for VIIRS band M1. This panel also includes a spectrally flat radiance with a value of unity.

The bandwidths for the RSRs, calculated over their total responses using Eq. 4, are listed in Table 2. In general, the bandwidths agree at the 1 % level, except for band M1, where there is a significant disagreement on the short wavelength side of the central peak. The effects of the RSR differences have yet to be studied.

5. BROAD-BAND SOURCE-BASED RESPONSIVITY

For NPP VIIRS, the manufacturer used an integrating sphere, the SIS100, as a source of known spectral radiance for the absolute calibration of the visible and near infrared bands during TVAC testing. When combined with the SpMA-based RSRs, the sphere radiances are used to calculate band-average spectral radiances for each of the bands,

$$L_{BNDAVG} = \frac{\sum_{\lambda=390}^{\lambda=1000} L_S(\lambda) R(\lambda) \Delta\lambda}{\sum_{\lambda=390}^{\lambda=1000} R(\lambda) \Delta\lambda}, \tag{6}$$

where $L_S(\lambda)$ is the sphere radiance at wavelength, λ, with units of W m^{-2} sr^{-1} μm^{-1}, and $R(\lambda)$ is the relative spectral response, dimensionless. The band-averaged spectral radiance, L_{BNDAVG}, has the same units as the sphere spectral radiance. It is the calculated absolute radiance over the entire band, since the values of $L_S(\lambda)$ in the equation are the known radiances from the sphere at each wavelength. These band-averaged spectral radiances are combined with the DNs from the instrument when measuring the sphere to provide band responsivities with units of DN (W m^{-2} sr^{-1} μm^{-1})$^{-1}$. The uncertainty requirement for these responsivities from the TVAC calibration is 5 % or less. This is the requirement for the MODIS instruments as well. We have no knowledge of the actual uncertainty estimate for the broadband radiances in Eq. 6, so we use the requirement from the instrument specifications in its place.

The TVAC-based responsivities have been calculated by the NPP Instrument Characterization Support Team (NICST) at NASA's GSFC for three instrument temperature plateaus during TVAC testing[7]. The responsivities, called gains by NICST, vary by less than 1 % for the three plateaus. Here we use the gains for the hot plateau in TVAC, which most closely duplicates the conditions for the SIRCUS test at BATC. Those gains (responsivities) are listed in Table 3. They have been calculated on a per-band basis. They are not given for each detector in the band[7]. They are designated "NICST" to reference the source of their calculation.

Table 3. Band responsivities from the TVAC testing of NPP VIIRS. These values were provided by NICST (see text for details). They are compared with the SIRCUS-based band responsivities in Table 3 from the special test at BATC. The differences are NICST from SIRCUS. The center wavelengths come from Table 1.

VIIRS Band	Center Wavelength (nm)	NICST Responsivity (DN W^{-1} m^2 sr μm)	SIRCUS-based Responsivity (DN W^{-1} m^2 sr μm)	Difference (%)
M1	410.6	27.3	20.5566	32.8
M2	443.6	23.9	22.6768	5.4
M3	486.4	27.5	25.8734	6.3
M4	550.8	37.1	35.2593	5.2
M5	671.6	51.0	53.4138	-4.5
M6	745.6	84.0	83.2178	0.9
M7	862.1	109.	110.0628	-1.0

The differences in the table are greatest at 411 nm and generally decrease with increasing wavelength into the near infrared at 746 nm and 862 nm. We believe the largest difference, for the 411 nm band, comes from the relatively large out-of-band response for the band (see Fig. 2b) combined with the shape of the sphere spectrum used for the calibration in TVAC. Compared to the amount at 411 nm, the sphere radiance is a factor of 6 greater at 560 nm, a factor of 10 greater at 730 nm, and almost a factor of 14 greater at 1000 nm. The effect of source spectral shape, combined with out-of-band response is dramatic for the calibration of NPP VIIRS. It is also significant for the source spectra that will be measured on orbit.

6. EFFECTS OF SOURCE SPECTRAL SHAPE

The individual SIRCUS ASRs have units of DN per unit radiance at each wavelength. When interpolated to uniform wavelength intervals and integrated (see Eq. 2), the responsivity becomes an unweighted sum over the wavelength range of the ASRs. In other words, each point has an identical weighting of unity. This is equivalent to the response to a source with a constant radiance of unity over all wavelengths. The calculations presented here use band-averaging, plus the ASR of the band, plus a normalized source radiance spectrum to calculate a weighting factor for each source spectral shape. To incorporate the SIRCUS-based responsivities into this methodology, we use the concept of a spectrally flat source with a value of unity. This said, alternate methodologies may exist that do not require the concept of a spectrally flat source.

For measurements of sources that are not spectrally flat, there must be some knowledge of the spectral shape of the source that is measured. For NPP VIIRS, the manufacturer used an integrating sphere, the SIS100, for its calibration. The actual spectral radiance for the VIIRS calibration has not been reported. Indeed, to cover the seven visible and near infrared bands, it is probable that more than one sphere radiance spectrum was used to provide several sphere brightness levels for the calibration. As a proxy for these spectra, we use a published radiance spectrum from the SIS100 when it was validated using transfer radiometers in the past[5]. That sphere, the SIS100, was used for the calibration of the MODIS instruments on NASA's Terra and Aqua platforms. Although the radiance spectrum we use is from the sphere used to calibrate NPP VIIRS, it is a spectrum from the past. Still, we feel it has a spectral shape that is close to those for the NPP VIIRS measurements in TVAC. A portion of its calibrated radiance spectrum[5], covering wavelengths from 300 nm to 1000 nm, is shown in Fig. 11a. It is the SIS100 radiance with ten 200 W, nine 45 W, and four 8 W lamps illuminated, SIS[10,9,4]. The greatest relative change in sphere radiance with wavelength occurs in the blue portion of the spectrum. The SIS[10,9,4] spectrum, normalized for VIIRS band M1, is shown in Fig. 11b.

Our initial normalization technique used the center wavelengths for the VIIRS bands as the normalization reference. These wavelengths, listed in Table 1, are band-averaged over the in-band responses of the bands. The technique normalizes each reference spectrum to unity at that wavelength. However, this normalization technique fails for radiance spectra with structure within the in-band wavelength region (see Section 7). Here we use an alternate approach by calculating the band-averaged spectral radiances for the reference spectra over the in-band responses of the bands. In the current approach, Eq. 6 is used, except that summation limits are the 1 % response points for the band, that is, the wavelengths where the response of the band is 1 % of the peak response or greater. The band-averaged spectral radiance from the calculation is used as the reference, L_{REF}, in place of the radiance at the center wavelength from the original technique. For band M1 and the sphere radiance spectrum in Fig. 11a, L_{REF} is 41.3 W m^{-2} sr^{-1} μm^{-1} at 411.5 nm. The normalized radiance, $L_N(\lambda)$ (dimensionless), is calculated as

Table 4. Band-average weighting factors for the VIIRS bands. The SIRCUS-based ASRs and two weighting functions are used for the calculations. The functions are a spectrally flat source of unity radiance and a source with the shape of an integrating sphere (SIS[10,9,4], see text for details).

VIIRS Band	F_{BND} Flat Shape (dimensionless)	F_{BND} SIS[10,9,4] Shape (dimensionless)	Difference (%)
M1	1.0000	1.2621	26.2
M2	1.0000	1.0310	3.1
M3	1.0000	1.0318	3.2
M4	1.0000	1.0083	0.8
M5	1.0000	0.9963	-0.4
M6	1.0000	0.9979	-0.2
M7	1.0000	0.9992	-0.1

Table 5. Band responsivities for the VIIRS bands. The responsivities are calculated using the numerator of Eq. 8 and the weighting functions in Table 3. The differences of the SIS-weighted responsivities from the spectrally-flat responsivities are identical to those in Table 3.

VIIRS Band	Responsivity Flat Shape (DN W^{-1} m^2 sr μm)	Responsivity SIS[10,9,4] Shape (DN W^{-1} m^2 sr μm)	Difference (%)
M1	20.5566	25.9442	26.2
M2	22.6768	23.3793	3.1
M3	25.8734	26.6973	3.2
M4	35.2593	35.5526	0.8
M5	53.4138	53.2169	-0.4
M6	83.2178	83.0404	-0.2
M7	110.0628	109.9799	-0.1

$$L_N(\lambda) = \frac{L(\lambda)}{L_{REF}}. \tag{7}$$

This is used to calculate a weighting factor that is band-averaged over the total response of the VIIRS band,

$$F_{BND} = \frac{\sum_{\lambda=390}^{\lambda=1000} L_N(\lambda) ASR(\lambda) \Delta\lambda}{\sum_{\lambda=390}^{\lambda=1000} ASR(\lambda) \Delta\lambda}, \tag{8}$$

where F_{BND} is the band-averaged weighting factor (dimensionless). For a constant radiance spectrum of unity, F_{BND} is unity as well. The numerator of Eq. 8 duplicates the calculation of the band responsivity in Eq. 2, plus the addition of the weighting factor.

The weighting factors from these calculations are listed in Table 4. For band M1 and the SIS[10,9,4] spectral shape, F_{BND} is about 26 % greater than unity. This comes from the relatively large out-of-band response on the red side of the band center (see Fig. 2b), combined with the shape of the source, which peaks near 1000 nm at a level more than an order of magnitude greater than at 411 nm.

The influence of $L_N(\lambda)$ in Eq. 8 is found only in the weighting of the ASR in the numerator. Figure 12a shows the ASR spectrum for band M1 interpolated to 0.1 nm intervals. Figure 12b shows the two radiance spectra used to provide normalized weighting factors for the band. Figure 12c shows the product of the ASR in Fig. 12a and the normalized radiances in Fig. 12b. Figure 12d shows summations of the weighted ASRs in Fig. 12c moving from 390 nm to 1000 nm. At the far right of Fig. 12d, these summations give the band responsivities for the two spectral shapes. The nearly vertical line near 410 nm in Fig. 12d shows the contribution of the central ASR peak in Fig. 12c. From 420 nm to 1000 nm, the summation for the spectrally flat source increases only slightly. For the SIS[10,9,4] source, there are significant contributions to the summations at wavelengths greater than 600 nm. For these wavelengths, the out-of-band contributions for the two weighted ASRs in Fig. 12c are noticeably different. The cause of the differences from the two weighted radiances lies away from the central peak of the ASR at 411 nm.

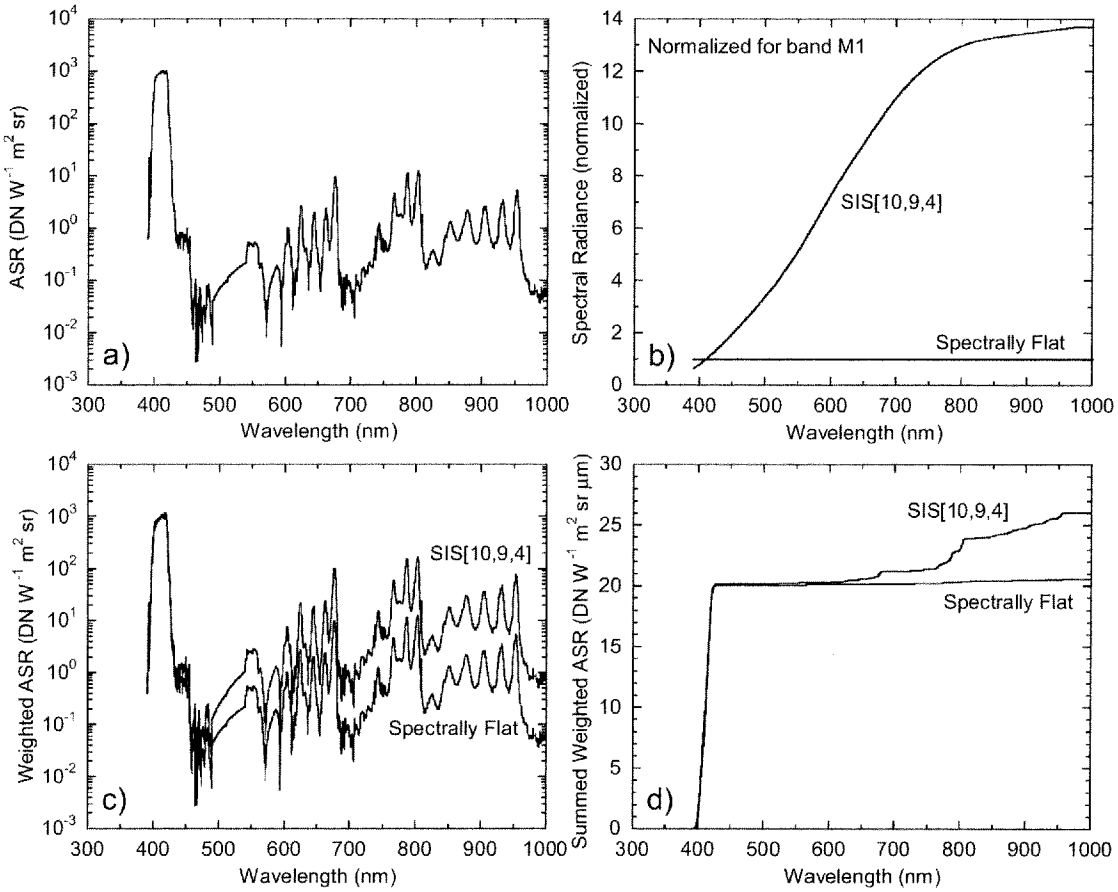

Figure 12. Effects of source spectral shape on VIIRS band M1. These effects are calculated using Eq. 8.

a) ASR spectrum from Fig. 1b interpolated to 0.1 nm intervals.

b) Two normalized radiance spectra, one for a spectrally flat source and one for the SIS100 with ten 200 W, nine 45 W, and four 8 W lamps illuminated, SIS[10,9,4].

c) The products, on a wavelength-by-wavelength basis, of the spectra in Figs. 12a and 12b.

d) The summations of the spectra in Fig. 12c. The sums at 1000 nm give the band responsivities for the two spectra.

Table 5 lists the weighted band responsivities calculated with the numerator of Eq. 8 for VIIRS bands M1 through M7. The percent differences between the two normalized radiances are the same as those in Table 4. The difference in the band responsivities for band M1 indicates that the band will produce significantly more DNs for a sphere weighted source than for a spectrally flat source when both sources have the same radiance near 411 nm.

For the SIRCUS-based measurements, the band responses are the same as those for a spectrally flat source. They have F_{BND}'s of unity. For other source spectral shape it is possible to multiply the responsivity from SIRCUS by the F_{BND} for that spectral shape to calculate the SIRCUS-based responsivity for that spectral shape. This has been done in Table 6, where the SIRCUS-based responsivity from Table 1 has been multiplied by the F_{BND} for the SIS[10,9,4] source to give the SIRCUS-based responsivity for the SIS[10,9,4].

The NICST band responsivities are also listed in Table 6, where they are compared with the SIRCUS responsivities after weighting for the F_{BND} for the SIS[10,9,4] source spectral shape. For band M1 there is a dramatic reduction in the difference. For bands M2, M3, and M4, there are also significant decreases. Here, the two sets of responsivities agree at the 5 % level. This is the uncertainty goal for the radiance calibration of NPP VIIRS. It should be noted that the SIS[10,9,4] spectral shape is not identical to those used for the TVAC testing of NPP VIIRS. Although it is from the

Table 6. Band responsivities from the TVAC testing of NPP VIIRS, provided by NICST. These responsivities are the same as in Table 4. They are compared with the SIRCUS-based responsivities from Table 3 weighted by the F_{BND} values for a source with the spectral shape of the SIS[10,9,4] integrating sphere in Table 6.

VIIRS Band	Center Wavelength (nm)	NICST Responsivity (DN W^{-1} m^2 sr μm)	Responsivity SIS[10,9,4] Shape (DN W^{-1} m^2 sr μm)	Difference (%)
M1	410.6	27.3	25.9442	5.2
M2	443.6	23.9	23.3793	2.2
M3	486.4	27.5	26.6973	3.0
M4	550.8	37.1	35.5526	4.4
M5	671.6	51.0	53.2169	-4.2
M6	745.6	84.0	83.0404	1.2
M7	862.1	109.	109.9799	-0.9

same sphere that calibrated NPP VIIRS in TVAC, it is only a proxy for them. As such, the corrections shown here are only approximations of those with the actual sphere spectral shapes for the NPP VIIRS calibration.

The source spectral shape correction scheme presented here can also be applied to the NICST band responsivities using the SpMA-based relative spectral responses in Figs. 9 and 10. The methodology is the same; however, there are differences between the SpMA-based and SIRCUS-based spectral responses. The effects of those differences have yet to be studied.

7. ON-ORBIT RADIANCE SPECTRA

A source with the spectral shape of the radiance from a lamp-illuminated integrating sphere does not accurately represent radiance spectra viewed on orbit, nor does the source inherent in SIRCUS-based calibrations. Consequently, the laboratory-based calibration coefficients based on the laboratory shapes, including the out-of-band effects inherent in those shapes, may have limited applicability on orbit. The band-averaged weighting factors from Section 6 provide a means of reducing errors based on source spectral shape in on-orbit measurements. These factors require knowledge of the spectral shapes found on orbit. Figure 13 shows four nominal top-of-the-atmosphere (TOA) radiance spectra[9]. Figure 13a shows the radiance spectrum from a diffuse reflecting panel illuminated by the Sun. For Fig. 13a, the diffuser has an albedo of 0.1, and the solar irradiance comes from the measurements of Thuillier et al.[9] For the VIIRS bands in the visible and near infrared, the fundamental on-orbit measurement is reflectance, which is the ratio of the upwelling Earth radiance to the radiance from the solar diffuser. The spectrum from the VIIRS solar diffuser is integral to each measurement by the VIIRS visible and near infrared bands. Figures 13b, 13c, and 13d give nominal TOA radiance spectra for oceans, grasslands, and deserts, respectively. These panels show the spectra with and without the effects of atmospheric trace gas absorption[8]. The VIIRS bands are set into atmospheric transmittance windows, that is, wavelength regions where atmospheric trace gas absorbances are minimal. For the calculations of source spectral effects in this section, the spectra without trace gas absorption are used.

In Section 6, concerns were raised about the normalization of radiance spectra to a band's center wavelength for source spectral shape corrections, particularly for sources with spectral structure. Here we use VIIRS band M3 and the spectrum of a solar-illuminated diffuser to demonstrate those concerns. Figure 14 shows the in-band portion of the ASR for VIIRS band M3, along with the solar diffuser spectrum over the same wavelength range. Both the diffuser and flat spectra in Fig. 14b are normalized to unity at 486.4 nm, the center wavelength for the band. For most of Fig. 14b, the normalized diffuser radiance lies well above the unity. This makes for a poor normalization to unity and a significant offset in the derived value for F_{BND}. When band-averaged over this wavelength range, the normalized solar diffuser spectrum in Fig. 14b has a value of about 1.11. This type of effect is the reason that the weighting functions in Section 5 are normalized over the in-band response of each band and not to the center wavelength.

The band-averaged weighting factors (F_{BND}'s) for the four spectra in Fig. 13 and VIIRS bands M1 through M7 are listed in Table 7. For the SIRCUS-based band responsivities, the F_{BND} values are unity for each band. To calculate the SIRCUS-based band responsivity for band M1 and the spectral shape of the solar diffuser, the responsivity from Table 1 (20.5566 DN W^{-1} m^2 sr μm) is multiplied by the appropriate F_{BND} in Table 7 (0.9920). This follows the process used to

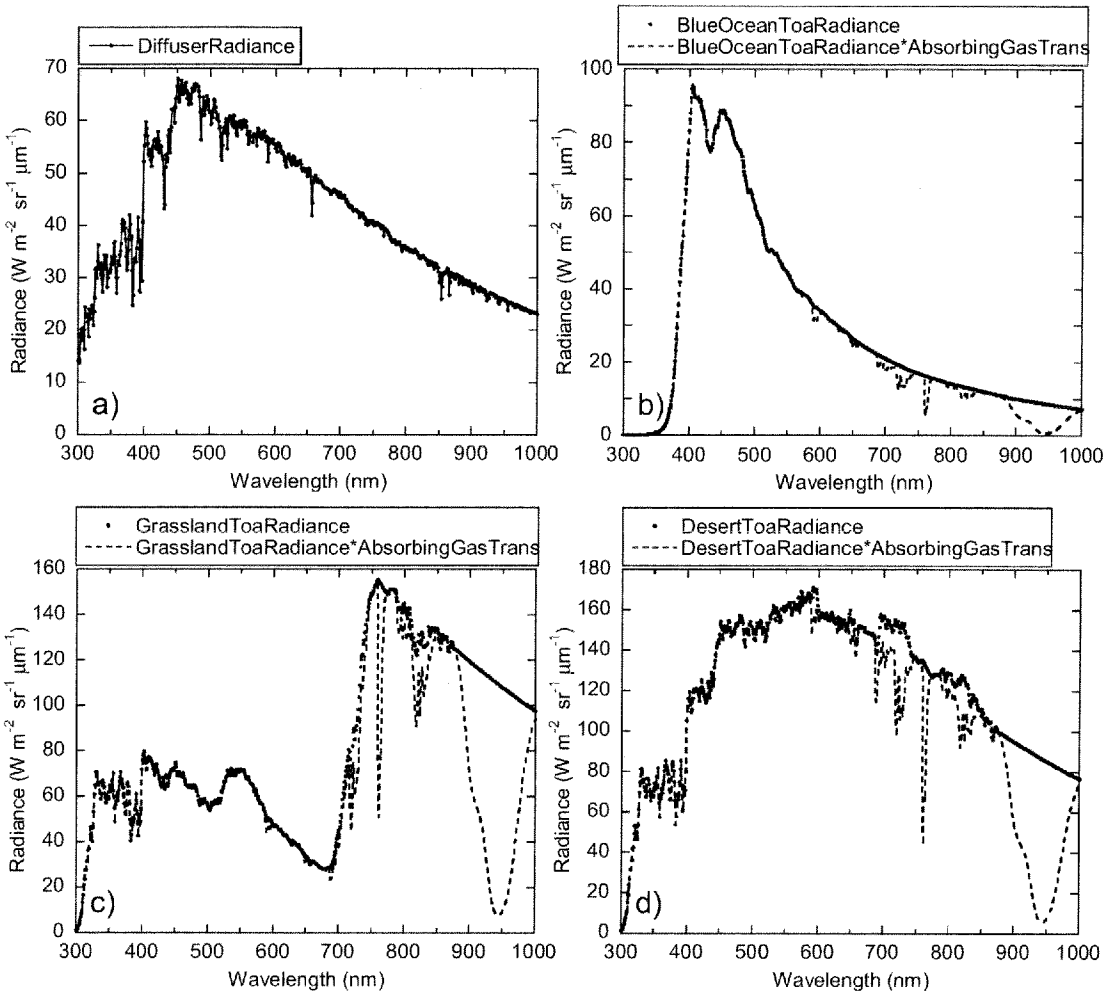

Figure 13. Four nominal top-of-the-atmosphere radiance spectra (Barnes and Butler, 2007).

a) Radiance spectrum for a solar diffuser on orbit. It is for the solar irradiance scattered by a diffuser with an albedo of 0.1.

b) Top-of-the-atmosphere radiance above a blue ocean. The symbols give the radiance without the effects of atmospheric trace gas absorption. The dashed lines include these atmospheric effects. The spectra without the trace gas absorption features are used in the band responsivity calculations.

c) Top-of-the-atmosphere radiance above a grassland.

d) Top-of-the-atmosphere radiance above a desert.

calculate the SIRCUS-based responsivities weighted by the SIS[10,9,4] spectrum in Table 6. The values for F_{BND} in Table 7 are only as good as the ASRs and the normalized radiance spectra used to calculate them. Those normalized spectra are based on the nominal spectra in Fig. 13. As such, the F_{BND} weighting factors and the responsivities calculated from them are only approximations to the actual values for NPP VIIRS on orbit. However, they do provide reasonable estimates for the spectral shape effects on NPP VIIRS measurements of Earth-exiting radiances.

Two of the F_{BND} values in Table 7 differ from unity by two percent or more. The first is the band-averaged weighting factor for blue oceans for band M1. The ocean spectrum in Fig. 13b has a peak near 410 nm and falls by two-thirds at 600 nm and by four-fifths 800 nm. In this region, the out-of-band contribution for the ocean is much less than for the flat spectrum (see Fig 15). In this figure, the out-of-band response in the red and near infrared combines with the relative excess in radiance from the spectrally flat source at these wavelengths (see Fig. 15b) to give an increased band

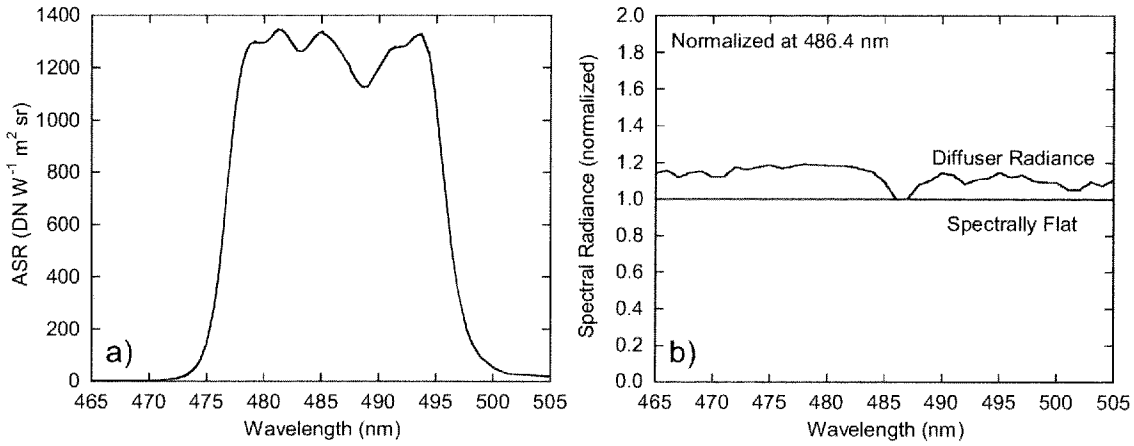

Figure 14. Band M3 ASR spectrum plus two normalized radiance spectra – spectrally flat and a diffuser illuminated by the Sun. The spectral shape for the diffuser radiance comes from the solar irradiance.

a) The ASR spectrum from Fig. 4a interpolated to 0.1 nm intervals.

b) Two radiance spectra normalized to unity at 486.4 nm, the band-average center wavelength for band M3. The diffuser radiance spectrum, before normalization, comes from Fig. 13a. This technique has been replaced by normalization of the band-average of the spectrum over the in-band response to provide L_{REF} in Eq. 7.

Table 7. Band-average weighting factors (F_{BND}'s) for the VIIRS bands. The reference spectral shapes come from Fig. 9. The band-average weighting factors from SIRCUS are unity. The band responsivities for these shapes are the products of the F_{BND} values and the SIRCUS-based band responsivities from Table 1.

VIIRS Band	F_{BND} Solar Diffuser Shape (dimensionless)	F_{BND} Blue Ocean Shape (dimensionless)	F_{BND} Grassland Shape (dimensionless)	F_{BND} Desert Shape (dimensionless)
M1	0.9920	0.9801	1.0109	1.0011
M2	0.9977	0.9949	1.0015	0.9996
M3	0.9955	0.9917	1.0077	0.9980
M4	0.9967	1.0039	1.0002	0.9966
M5	1.0005	1.0099	1.0400	0.9993
M6	1.0010	1.0074	0.9949	1.0001
M7	1.0010	1.0045	0.9992	1.0006

responsivity for this source. As a result, the F_{BND} for the spectrally flat source is 2 % greater than for the ocean. The second is the F_{BND} for grasslands for band M5. The center wavelength for this band, 672 nm, lies in the spectral valley in Fig. 13c with increased radiance at both lower and higher wavelengths. Hence, there is the 4 % increase in F_{BND} from out-of-band response relative to a spectrally flat source. For VIIRS band M7 at 862 nm, the grassland and desert radiances in Figs. 13c and 13d are approximately the same. For VIIRS band M5 at 672, those radiances in Figs. 13c and 13d differ significantly. As a result, the M5 to M7 radiance ratio provides an excellent means of distinguishing between grasslands and deserts. This use for band M5 outweighs the source spectral effect for the band when viewing grasslands at 672 nm. However, the methodology presented here provides a means for reducing that effect in grassland measurements.

As discussed above, the principal visible and near infrared measurements that VIIRS will provide on orbit are reflectances. Each reflectance measurement includes a radiance measurement of the solar diffuser. For reflectance measurements, the preferred source spectral shape for the VIIRS gains (band responsivities) will be that of the diffuser illuminated by the Sun (Fig. 13a). The band-averaged weighting factors in Tables 4 and 7 provide a means of converting both the NICST and the SIRCUS responsivities to those for the solar diffuser. However, the updated values from those two

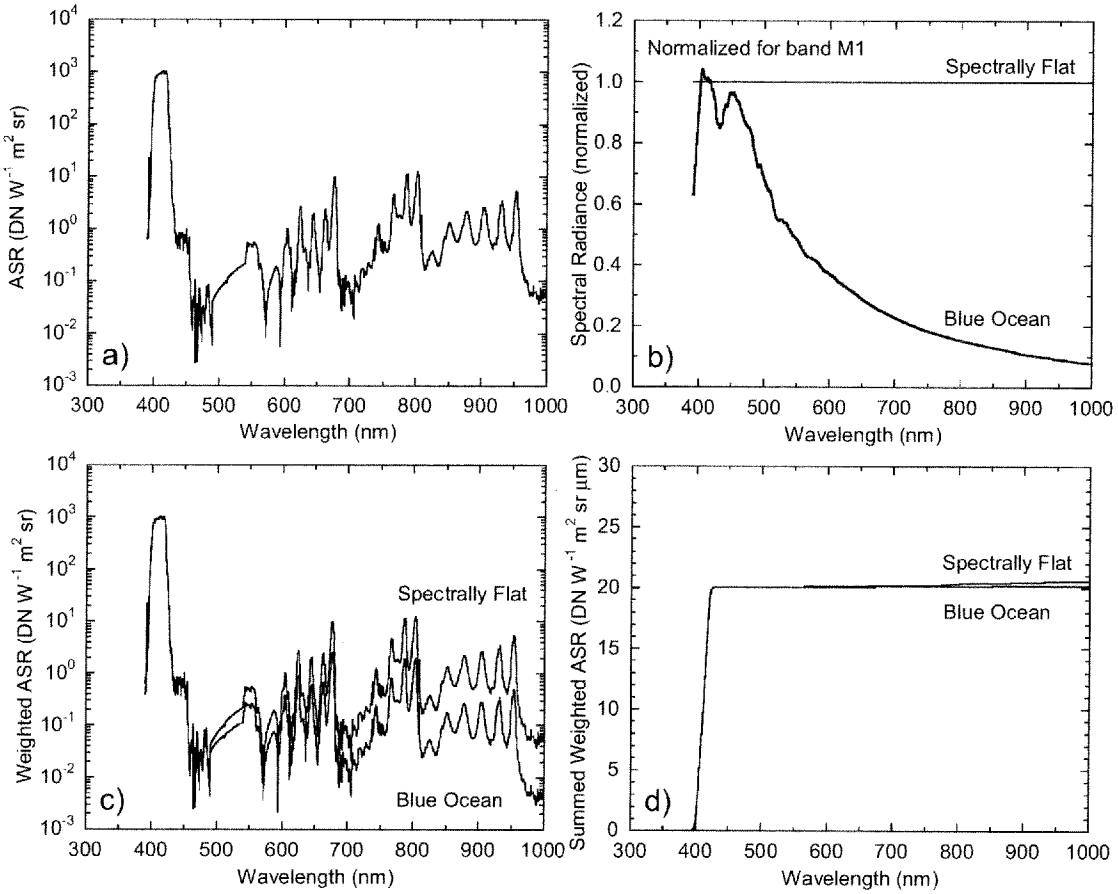

Figure 15. Effects of source spectral shape on VIIRS band M1. These effects are calculated using Eq. 8.
a) ASR spectrum from Fig. 1b interpolated to 0.1 nm intervals.
b) Two normalized radiance spectra, one for a spectrally flat source and one for the blue ocean top-of-the-atmosphere radiance.
c) The products, on a wavelength-by-wavelength basis, of the spectra in Figs. 15a and 15b.
d) The summations of the spectra in Fig. 15c. The sums at 1000 nm give the band responsivities for the two spectra.

tables will require the actual sphere spectral shapes for the TVAC testing of NPP VIIRS. For Earth-exiting radiances, the tables will require updated values as well.

The specified uncertainty for reflectance measurements from VIIRS on orbit is 2 %. From Table 7, the difference in the F_{BND} values for the solar diffuser and the ocean for band M1 is 1.2 %. In a like manner, the differences for the solar diffuser and grasslands are 1.9 % and 4.0 % for bands M1 and M5, respectively. For these cases, source spectral effects – if not properly accounted for – may expand the uncertainty for the reflectance measurements outside of the 2 % limit requirement.

8. CONCLUDING REMARKS

In early 2010, NPP VIIRS measured radiances from a SIRCUS source after the delivery of the completed instrument to the NPP spacecraft manufacturer's facility. The SIRCUS measurements were a special test of a new sensor-level calibration approach. SIRCUS provided a monochromatic source of known radiance over a broad range of wavelengths from an integrating sphere that overfilled the VIIRS entrance pupil. When combined with the outputs of the VIIRS sensor while viewing the radiance source, a set of absolute spectral radiance responses was generated. The uncertainties of the SIRCUS-based band responsivities are estimated to be 0.5 %.

Before the special test, NPP VIIRS was calibrated at the instrument manufacturer's facility. The calibration by the instrument manufacturer used a proven technique that has been employed for decades. In that calibration, the relative spectral response of VIIRS was measured using a lamp-illuminated monochromator as a source of light over narrow wavelength ranges. To provide absolute radiance responsivities, the instrument also measured the radiance from a calibrated lamp-illuminated integrating sphere. The uncertainty budget for the instrument manufacturer's radiance calibration is unknown to us. As a result, we use the 5 % uncertainty requirement from the instrument specifications in its place. Uncorrected for source spectral shape, comparisons showed differences between the two sets of band responsivities ranging from 32.8 % for band M1 to -4.5 % for band M5.

The effect of source spectral shape caused by the sensor's out-of-band response is a major contributor to the differences in the laboratory calibrations. When a correction for source spectral effects is applied to the comparison of the SIRCUS and TVAC calibrations, the difference for band M1 is reduced from 32.8 % to 5.2 % and the differences from the other bands are within the 5 % uncertainty requirement for the instrument. The corrections used here are only as good as the ASRs and the SIS spectrum used in their calculation. The SIS[19,9,4] spectrum comes from measurements of the sphere used to calibrate NPP VIIRS; however, it is not identical to the actual radiances used in that calibration. Thus, the correction is only an approximation to the real one. Still, the results presented here are an indication of the requirement to include the source spectral shape when comparing SIRCUS and vendor results.

The effect of source spectral shape caused by the sensor's out-of-band response is also a major contributor to the on-orbit performance of NPP VIIRS. On orbit, the instrument will not measure radiance spectra with the shape of an integrating sphere's output. Since NPP VIIRS will produce reflectances from its visible and near infrared bands on orbit, the reference spectral shape for the calibration of those bands should be that of a diffuser illuminated by the Sun. Measurements of upwelling Earth radiances will be ratioed to radiances from the onboard diffuser to produce reflectances. The uncertainty requirement for those reflectances from NPP VIIRS is 2 %. Nominal TOA radiance spectra for oceans, grasslands, deserts, and an onboard solar diffuser have been used to calculate weighting factors for the VIIRS visible and near infrared bands. The weighting factors show source spectral shape differences of up to 4 % from the SIRCUS calibration. If the source spectral shape of the diffuser is used as a reference, the spectral effects are still as large as 4 % for certain bands and Earth scenes. These estimated effects are only as good as the nominal TOA radiance spectra used to calculate them. However, for these cases, source spectral effects may expand the uncertainty for the VIIRS reflectances outside of the 2 % limit in the instrument's requirements.

For future instruments with SIRCUS-based calibrations in the laboratory, source spectral effects on orbit may be significantly greater than the 0.5 % uncertainty for the laboratory calibration. As shown for NPP VIIRS, these effects are caused by significant responses in the bands away from the central response peaks, that is, by out-of-band responses. The solution for the effects of source spectra is strict limiting of the out-of-band response in the instrument. However, it is possible to use on-orbit measurements from the set of instrument bands to calculate, and correct for, the residual effects of source spectral shape dependence (see chapter 2 of ref. 10 and section 3 of ref. 8). Such a technique provides the potential for a measurement-by-measurement correction, rather than a limited set of corrections based on nominal spectra.

9. ACKNOWLEDGEMENTS

The authors wish to thank Bob Lambeck from the QSS Group, Frank DeLuccia from the Aerospace Corporation, Craig Kent from Stellar Solutions, Tom Gonzales from Ball Aerospace, and Chris Moeller from the University of Wisconsin for their work during the SIRCUS measurements at BATC.

REFERENCES

1. Schueler, C., Clement, J. E., Darnton, L., DeLuccia, F., Scalione, T., and Swenson, H., "VIIRS sensor performance," International Geosciences and Remote Sensing Symposium (IGSRSS) Proceedings, July 2003.
2. Scalione, T., DeLuccia, F., Cymerman, J., Johnson, E., McCarthy, J. K., and Olejniczak, D. "VIIRS Initial performance Verification," International Geosciences and Remote Sensing Symposium (IGSRSS) Proceedings, July 2005.
3. Murphy, R., Barnes, W., Lyapustin, A., Privette, J., Welsch, C., DeLuccia, F., Swenson, H., Schueler, C., Ardanuy, P., and Kealy, P., "Using VIIRS to provide data continuity with MODIS," International Geosciences and Remote Sensing Symposium (IGSRSS) Proceedings, July 2001.
4. Schueler, C., Clement, J. E., Ardanuy, P., Welsch, C., DeLuccia, F., and Swenson, H., "NPOESS VIIRS sensor design overview." Proc. SPIE, 4483, 11-23, 2002.
5. Butler, J. J., Johnson, B. C., Brown, S. W., Saunders, R. D., Biggar, S. F., Zalweski, E. F., Markham, B. L., Gracey, P. N., Young, J. B., and Barnes, R. A., "Radiometric measurement comparison on the integrating sphere source used

to calibrate the Moderate Imaging Spectroradiometer (MODIS) and the Landsat 7 Enhanced Thematic Mapper (ETM+)," J. Res. Natl. Inst. Stand. Technol, 108, 199-228, 2003.
6. Brown, S. W., Eppeldauer, G. P., and Lykke, K. R., "Facility for spectral irradiance and radiance responsivity calibrations using uniform sources," Appl. Opt., 45, 8218-8237, 2006.
7. Sun, J., and Che, N., "Summary of F1 radiometric performance for RSB from TV RC-02 tests," NICST_Memo_10_010, May 3, 2010.
8. Barnes, R. A., and Butler, J. J., "Modeling spectral effects in Earth-observing satellite instruments," Proc. SPIE, 6744, 64771K, 2007.
9. Thuillier, G., Hersé, M., Labs, D., Foujols, T., Peetermans, W., Gillotay, D., Simon, P. C., and Mandel, H., "The solar spectral irradiance from 200 to 2400 nm as measured by the Solspec spectrometer from the Atlas and Eureca missions," Solar Phys., 214, 1-22, 2003.
10. Barnes, R. A., Yeh, E-n, and Epplee, R. E., "SeaWiFS Calibration Topics, Part 1," NASA Technical Memorandum 104566, Vol. 39, 1996.